ATOMIC FORCE MICROSCOPY
Imaging/spectroscopy of Biological Membranes

Purple membranes

Light activation of these proteins modulates cellular excitability with millisecond precision

The so-called **Purple Membranes (PM)** are part of the membrane of the archaea Halobacterium salinarium, an extremophile naturally found in salt saturated water.
This particular biological membrane **contains only one protein, bacteriorhodopsin (bR) and about seven different unusual membrane lipids** assembled in a hexagonal lattice of bR trimers (p3 crystallographic point group, 6.2 nm lattice constant).

C

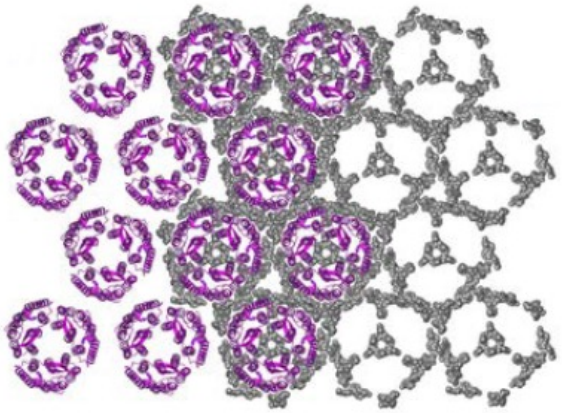

2D hexagonal lattice

The protein-lipid ratio has recently been determined to be **10 lipids per bR.**
The proteins represent 75% of PM mass and cover 50% of the membrane surface.
bR acts as a **light-driven vectorial proton pump** which converts photonic energy into a proton gradient across the membrane.
The induced electrochemical gradient is subsequently used by ATP-synthase as an alternative driving force to produce ATP in mediums particulary poor in oxygen.

The absorption spectrum of bR in its ground state (maximum absorbtion at 565 nm) is responsible for the purple colour of PM

B

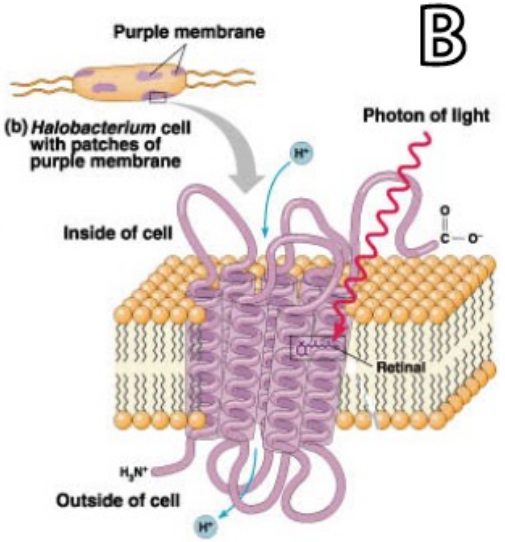

Purple membranes

PM is one of the best known biological membrane and an important model system to confront new theories and experimental methods.
bR was indeed the first integral membrane protein which structure was determined by X-ray crystallography of three-dimensional crystals grown in cubic lipid phase (non soluble proteins: difficulty in crystallization!)

N.B: membrane proteins are either peripheral (at the surface) and soluble in high ionic strenght acqueous solution (1 M salt) or integral, and can be solubilized only with detergent

All the protein membranes are coded by 20-30 % of the genome! But of all the known protein structures, only 5 % is of membrane proteins!

Purple membranes

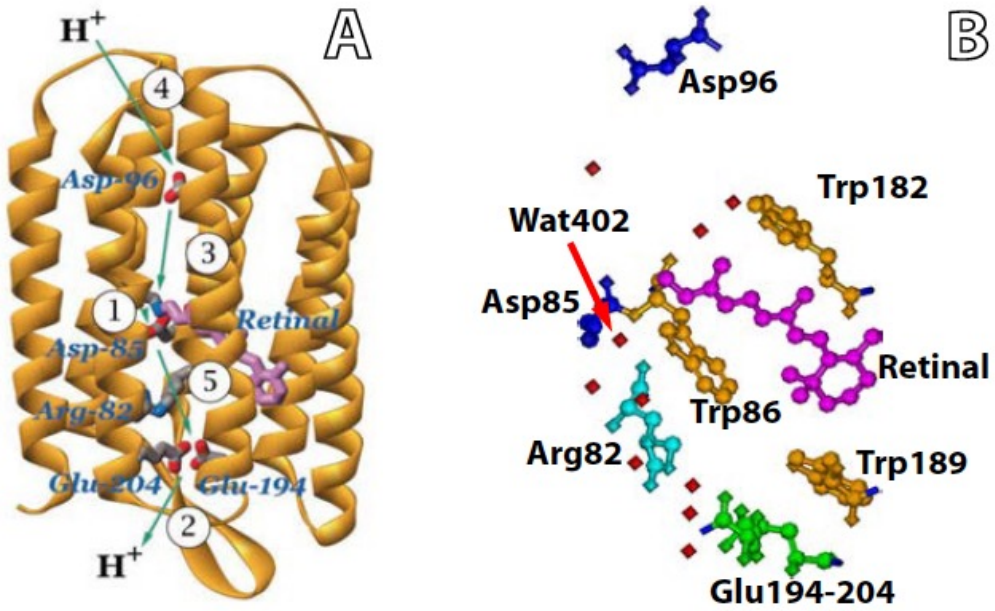

bR is an integral 26 KDa membrane protein composed 248 amino acids arranged in 7 transmembrane α-helices that surround a central cavity which encloses a chromophore, the retinal, linked to the protein backbone (Lys216 residue, helix G) via a Schiff base.

When the protein is in its fundamental/ground state (called bR state), the retinal chromophore adopts an all-trans configuration. Upon light absorption by the protein, the retinal can isomerize around its $C_{13} = C_{14}$ double bond, adopting a 13-cis configuration. This new chromophore conformation triggers a series of structural rearrangements in bR leading to the pumping of a proton from the inside to the outside of the archea.

Purple membranes

The isomerization of the retinal chromophore modify temporarily the position of charged residues within the protein allowing directional pumping of one proton over a **~ 10-20 ms photo-cycle**. The modifications of the retinal local electrical environment can be observed spectroscopically

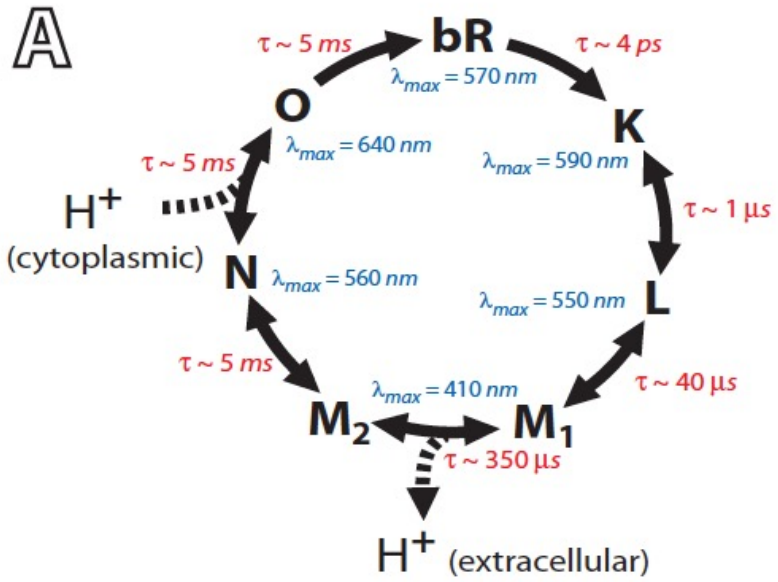

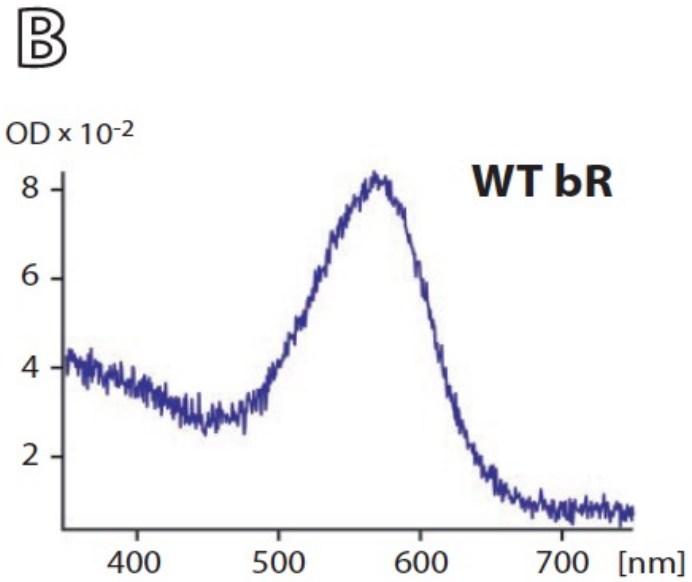

Purple membranes

In PM, **bR molecules lateral and rotational movements are prevented by the crystalline assembly**. PM is rather rigid with a viscosity typically 10^3-10^4 higher than that of halobacterial membrane lipids.

Within one trimer, the proximity between the bR molecules allows direct protein-protein interactions through the formation of salt bridges, hydrogen bonds and van der Waals interactions between the α-helices of the different proteins involved.

These interactions are however not sufficient to explain the important trimer stability in which specific protein-lipid interactions are involved. The exceptional cohesion within a single trimer is believed to be related to the protein activity through cooperativity.

Purple membranes

PM contains many different lipids some of which are not found in any other membrane and are necessary for bR activity, also in reconstituted membranes. To date, seven different lipids have been reported :
three phospholipds, two glycolipids, squalene and traces of vitamin MK8.

The requirement of a fixed membrane composition indicates that **selective interactions occur between bR and certain lipid molecules** and that these interactions are essential for lattice assembly and bR function.

Phospholipids represent ~ 40% of PM lipids. their head-group comports two negative charges which makes them particularly hydrophilic. Fluorescence studies have demonstrated that phospholipids are located mainly in PM cytoplasmic leaflet inter-trimer space.

Glycolipids represent ~ 30% of PM lipids. Unlike phospholipids, glycolipids show clear patterns in PM diffraction experiments suggesting that they are specifically and tightly bound to bR.

Local probe techniques have also been used to study purple membrane (Tamayo et al. 1995) and bR was **the first membrane protein extensively studied by atomic force microscopy and force spectroscopy.**

Purple membranes

Local probe techniques have also been used to study purple membrane (Tamayo et al. 1995) and bR was **the first membrane protein extensively studied by atomic force microscopy and force spectroscopy.**

The analogy between bR and **GPCR (G-protein** (mol. Switches) **coupled receptors)** is also an important factor contributing to the use of bR as a model system.

Unlike most of the prokaryotic α-helical membrane proteins which are composed of six or twelve transmembrane helices, **eukaryotic α-helical membrane proteins show a preference for seven transmembrane α-helices mainly because of the GPCRs**. The bR structure with seven transmembrane α-helices enclosing the active group is a characteristic of GPCRs. The first GPCR structure resolved, **bovine rhodopsin**, was achieved only recently and most of the previous pharmaceutical studies aiming at GPCR were based on the structure of bR. To date, the only GPCR structure resolved remains rhodopsin, a representant of the largest GPCR sub-family (A-family with 90% of GPCRs). Despite the fact that bR is not a GPCR, it is related to rhodopsins and remain an important model for pharmacological studies.

Purple membranes

G protein-coupled receptors (**GPCRs**), also known as **seven-(pass)-transmembrane domain receptors**, and **G protein-linked receptors** (**GPLR**), form a large group of evolutionarily related proteins that are cell surface receptors that detect molecules outside the cell and activate cellular responses. They are coupled with G proteins.

G proteins, also known as **guanine nucleotide-binding proteins**, are a family of proteins that act as molecular switches inside cells, and are involved in transmitting signals from a variety of stimuli outside a cell to its interior.

Their activity is regulated by factors that control their ability to bind to and hydrolyze guanosine triphosphate (GTP) to guanosine diphosphate (GDP). When they are bound to GTP, they are 'on', and, when they are bound to GDP, they are 'off'. G proteins belong to the larger group of enzymes called GTPases.

HR-AFM in membrane biology

High-resolution AFM has been applied to the imaging of bacterial membrane proteins, deriving the free energy landscape for domains within single protein mole

AFM

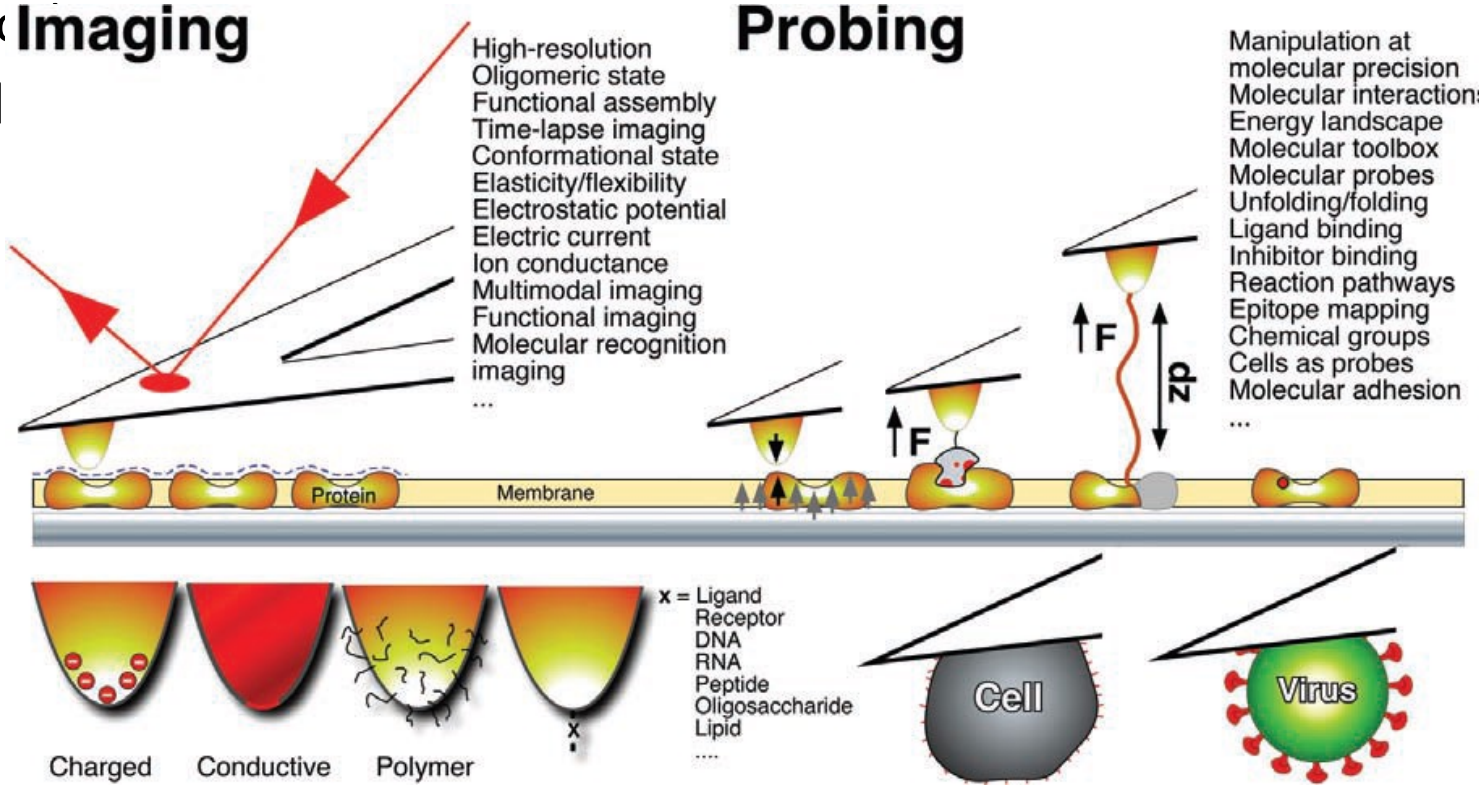

Imaging resolution in cell membranes: 10 nm
Imaging resolution in supported cell membranes: better than 1 nm (no fixing, labeling, Staining, room T, buffer solution)

S. Scheuring, D. Muller, H. Stalhberg, H.-A. Engel, A. Engel, *Eur. Biophys. J.* **31**, 172 (2002)

D.J. Muller et al. J. Mol. Biol. **(1999)** 285**, 1903-1909**

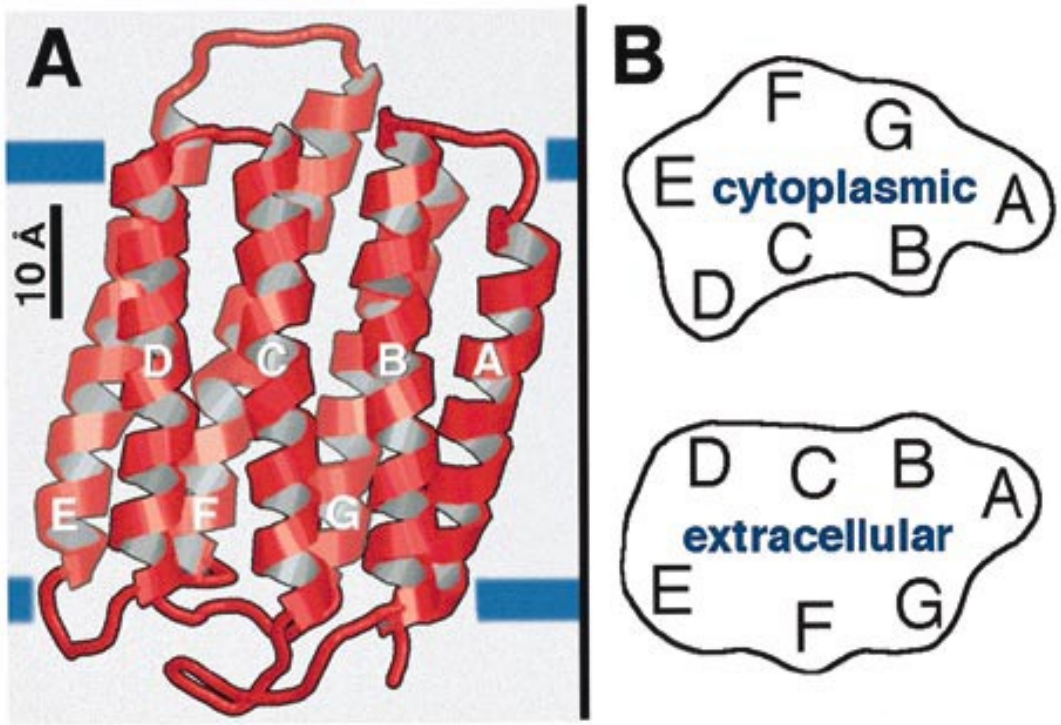

Structure of bacteriorhodopsin. (a) Ribbon representation as revealed by electron crystallography (Grigorieff et al., 1996). Because of their disordering, the N terminus of helix A and the C terminus of helix G were not resolved and the B-C loop was only partly resolved. Blue lines indicate the cytoplasmic and extracellular surfaces determined by Kimura et al. (1997).
(b) Outlines of 10 AÊ thick slices of the cytoplasmic and the extracellular BR surface.

D.J. Muller et al. / Biochimica et Biophysica Acta 1460 (2000) 27-38

PM reconstructed membrane on mica. Cytoplasmic vs. extracellular side

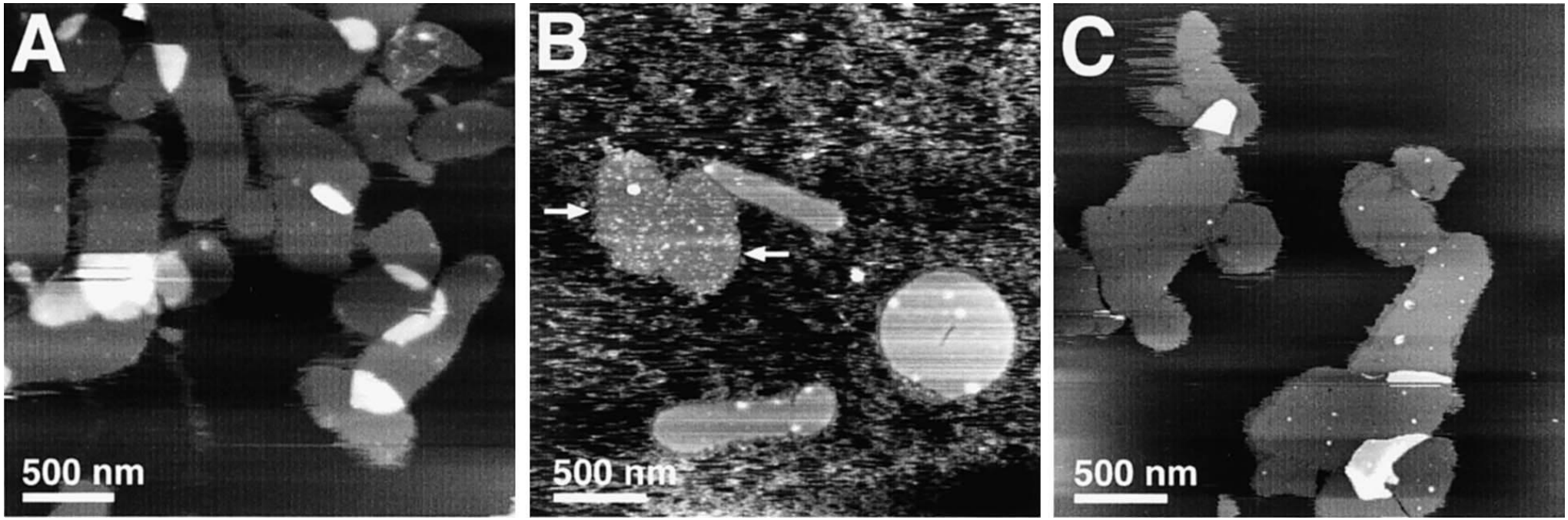

D.J. Muller et al. J. Mol. Biol. **(1999)** 285**, 1903-1909**

8.3(±1.9) Å **(**n . **398)**

6.4(±1.2) Å **(**n . **398)**

a=b=6.2±0.2 nm

The loops connecting the **alpha** -helices appeared to be disordered as they could not be resolved reliably.

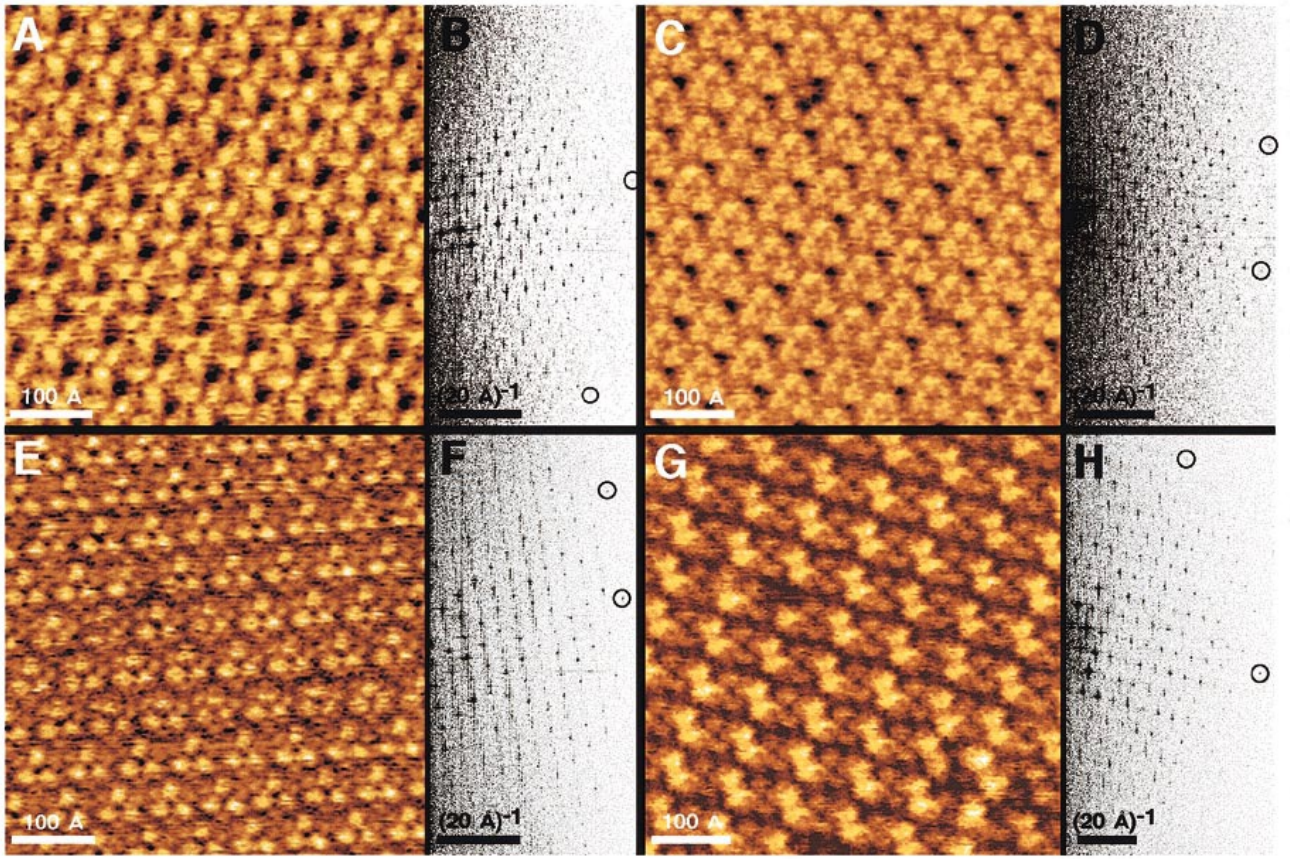

5.3(±0.7) Å **(**n . **320)**

in A protrusion arises from the loop connecting transmembrane **a** -helices E and F

(a) Native cytoplasmic surface recorded at 100 pN. (b) Power spectrum of (a). (c) Cytoplasmic surface recorded at 200 pN. (d). Power spectrum of (c). (e) Native extracellular surface recorded at 100 pN. (f) Power spectrum of (e). (g) Orthorhombic crystal of BR recorded at 100 pN. In this crystal form (p22121) the rows of BR dimers alternate, to expose either their cytoplasmic or their extracellular surfaces to the aqueous solution. (h) Power spectrum of (g).

N.B.: For the achievement of high resolution imaging a specific ionic concentration was required in order to balance van der Waals attractive forces with Electrostatic Double Layer repulsive forces (Muller & Engel 1997; Muller et al. 1999a).

Biochimica et Biophysica Acta 1460 (2000) 2738

Imaging of a statistically significant number of single proteins by AFM allows structural variability assessment and multivariate statistical classification to unravel the principal modes of the protein motion. arrangement of tripartite protrusions on a trigonal lattice (a = b = 6.2 +-0.2 nm) exhibiting a maximum height difference to the lipid membrane of 0.53+-0.07 nm.

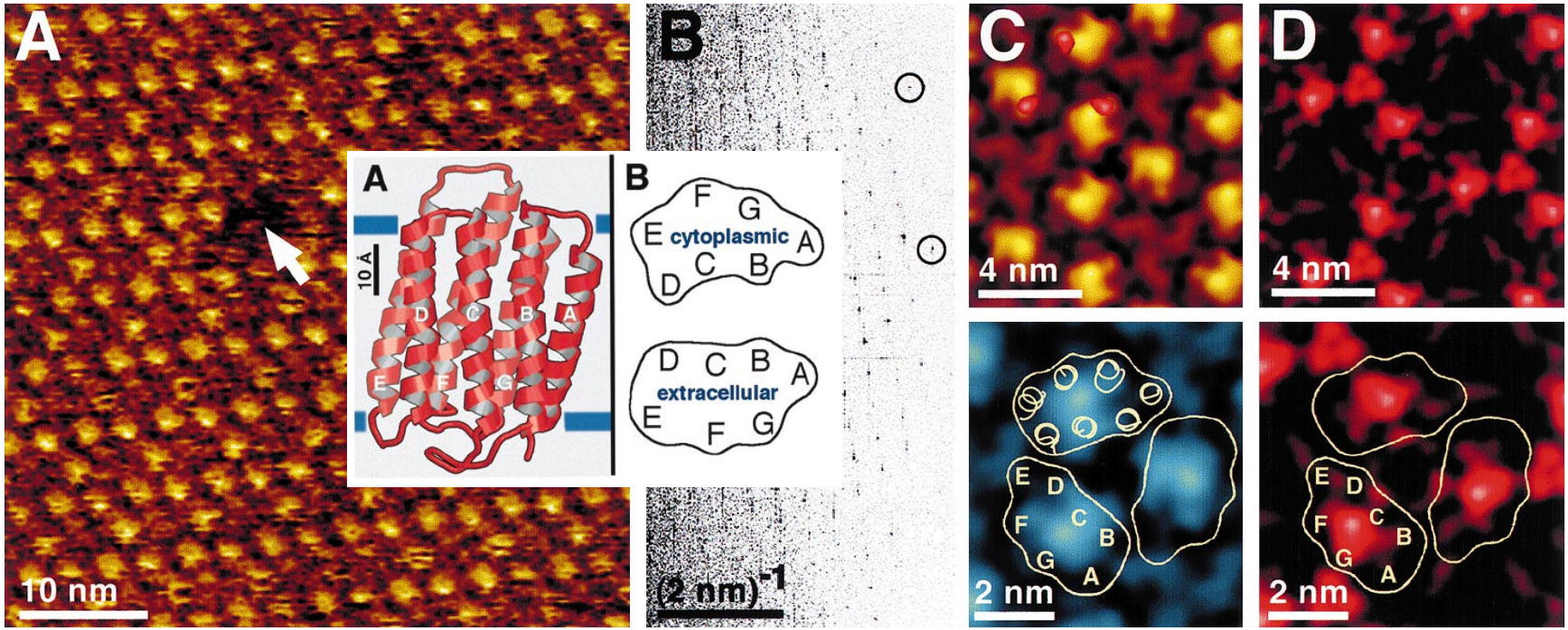

Extracellular purple membrane surface recorded in buffer solution (A). The PM surface exhibits a defect of the size of a BR trimer (arrow). (B) The power spectrum of A extends to the 11th order indicating a lateral resolution of 0.49 nm. (C) Averaged extracellular surface of the BR trimer (average of 320 unit cells). The correlation average is displayed in perspective view (top, shaded in yellow brown) and in top view (bottom, in blue) with a vertical brightness range of 1 nm and exhibited a 6.1% root-mean-square (RMS) deviation from three-fold symmetry.

Biochimica et Biophysica Acta 1460 (2000) 2738

Imaging of a statistically significant number of single proteins by AFM allows structural variability assessment and multivariate statistical classification to unravel the principal modes of the protein motion

Extracellular side

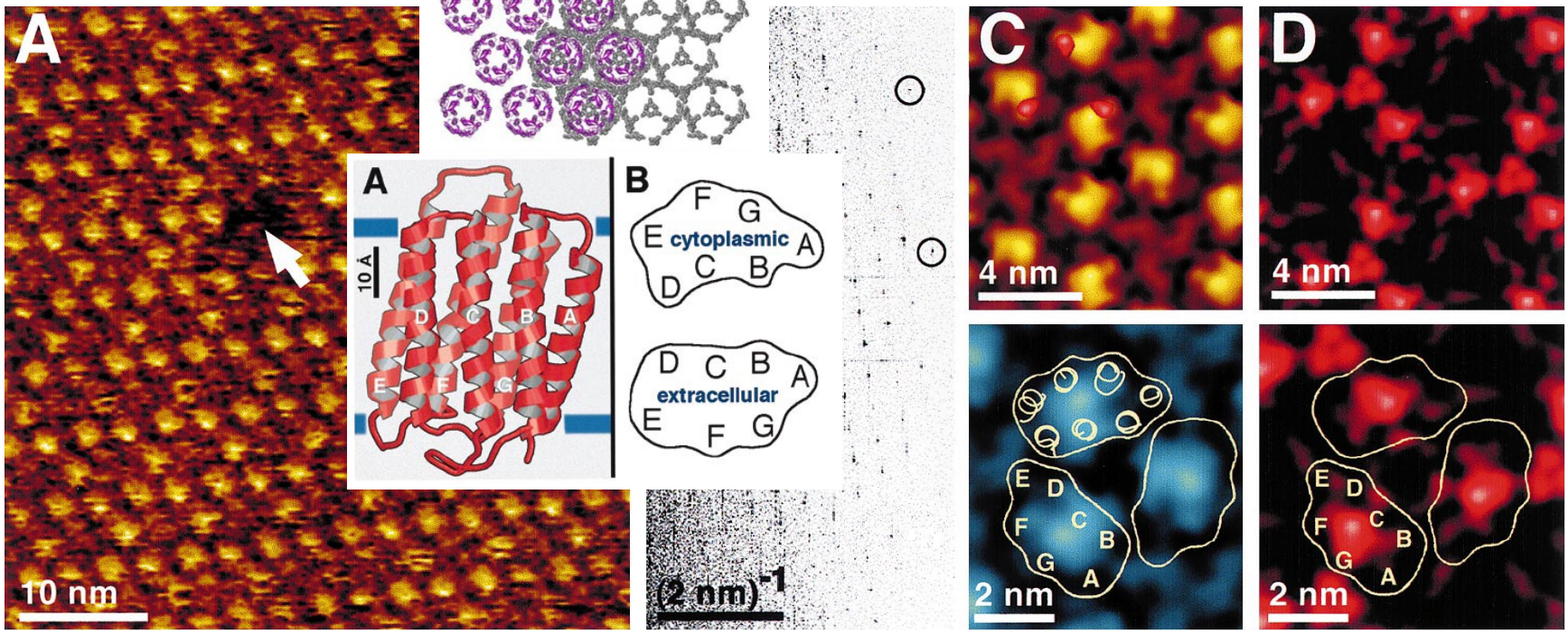

To assess the flexibility of the different structures, **standard deviation (S.D.) maps are calculated** (D) and had a range from 0.07 (lipid) to 0.12 nm (region of the FG loop). Surface regions exhibiting an S.D. above 0.1 nm are superimposed in red-to-white shades in top of C. The topograph was recorded in buffer solution (100 mM KCl, 10 mM Tris^ HCl, pH 7.8) at a loading force of 100 pN. The outlined BR trimer representing sections close to the extracellular surface of the lipid membrane was obtained after merging five atomic models of BR derived from electron and X-ray crystallography.

Biochimica et Biophysica Acta 1460 (2000) 2738

Imaging of a statistically significant number of single proteins by AFM allows structural variability assessment and multivariate statistical classification to unravel the principal modes of the protein motion

Extracellular side

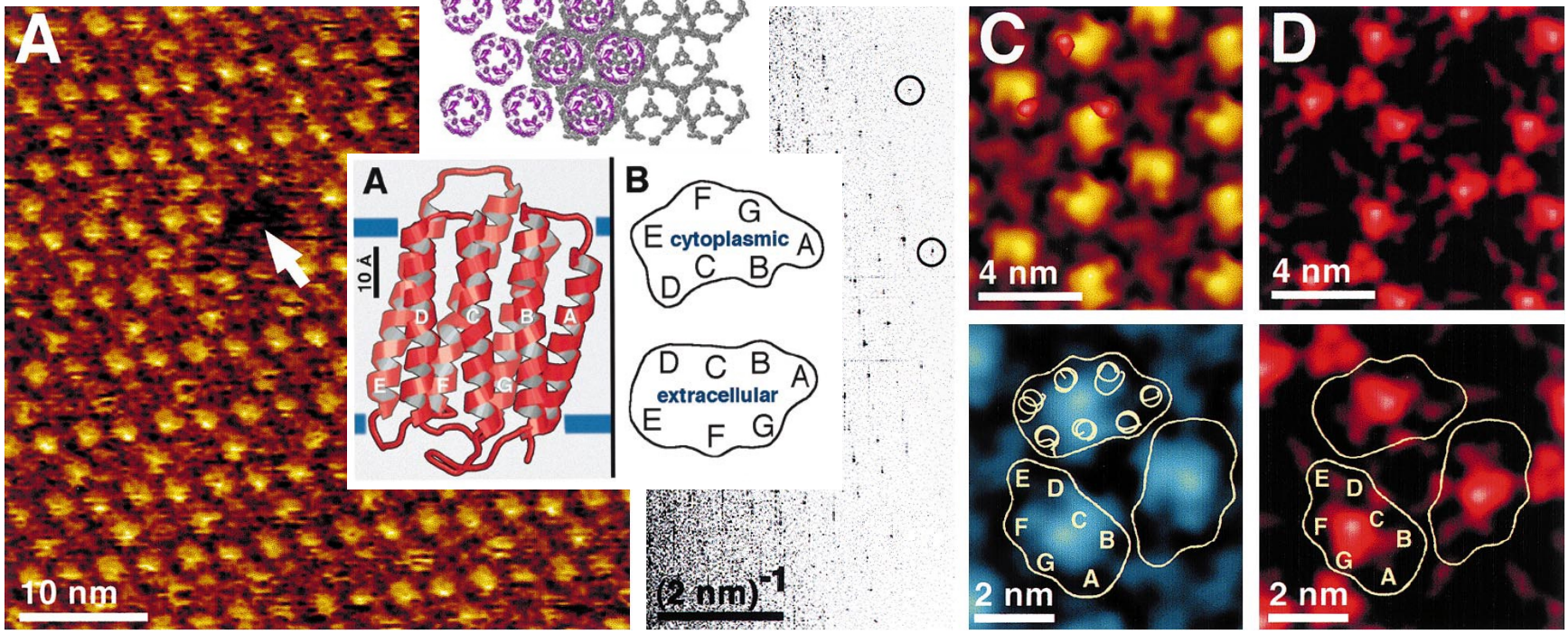

The most prominent protrusion is the L-hairpin in the BC loop connecting the transmembrane K-helices B and C. In the topograph, this protrusion is located between helices C and G. The shoulder near helix A is likely the N-terminus. Loop FG may contribute to the major protrusion, although it does not extend much above the lipid headgroups in the atomic models.

However, this area exhibits an enhanced standard deviation (S.D.) of 0.12 nm compared to the background (0.07 nm; Fig. 2D) indicating an increased structural variability and alternative conformations not reflected in the atomic models derived from electron and X-ray crystallography.

D.J. Muller et al. J. Mol. Biol. (1999) 285, 1903-1909 / Bioch. et Bioph. Acta 1460 (2000) 27-38

Pronounced protrusion extending 0.83 ¸ 0.19 nm above the lipid surface. This protrusion is associated with the loop connecting helices E and F

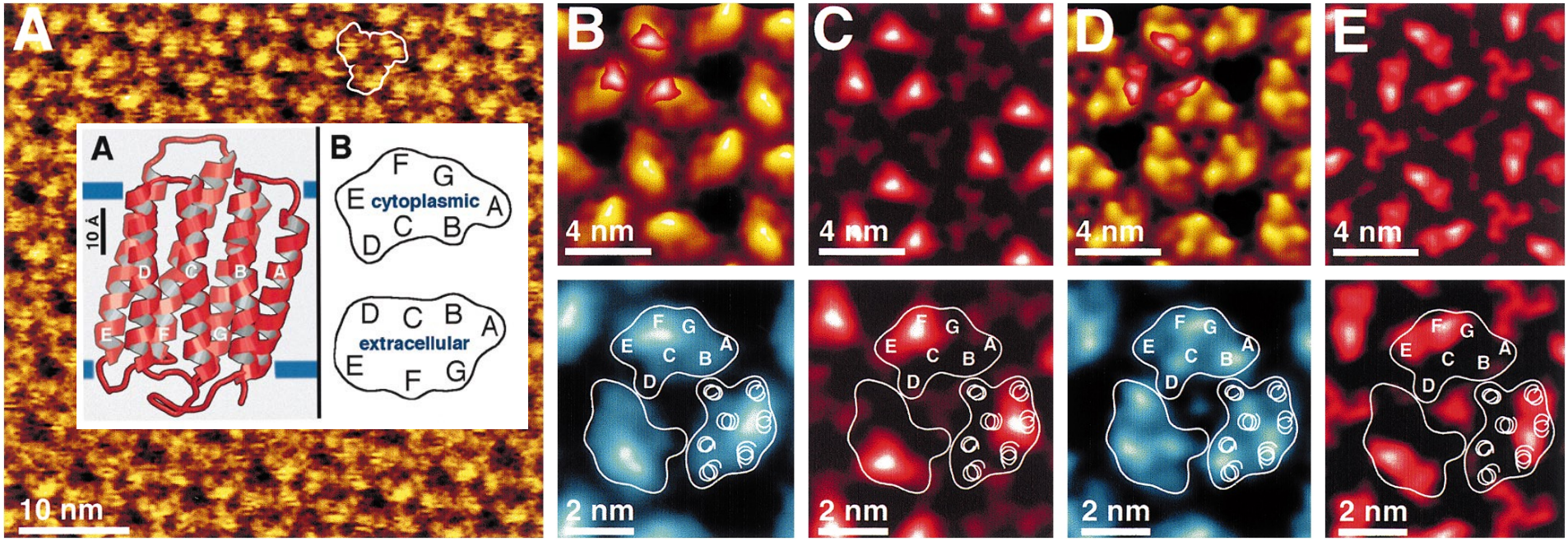

Fig. 3. Force-dependent surface topography of the **native cytoplasmic purple membrane surface**. (A) At the top of the image, the force applied to the AFM stylus was 100 pN. While scanning the surface line by line, the force was increased until it reached 150 pN at the bottom of the image. This force-induced conformational change of BR was fully reversible. Correlation averages of the cytoplasmic surface recorded at 100 pN (B) and at 200 pN (D). The correlation averages are displayed in perspective view (top, shaded in yellow brown) and in top view (bottom, in blue) with a vertical brightness range of 1 nm and exhibited 9.2% (B) and 14.1% (D) RMS deviations from three-fold symmetry. Structural flexibilities were accessed by S.D. maps (C and E corresponding to B and D, respectively) which had a range from 0.08 (lipid) to 0.19 nm (EF loop region). Surface regions exhibiting an S.D. above 0.12 nm are superimposed in red-to-white shades in the top of B and D. The topograph was recorded in buffer solution (100 mM KCl, 10 mM Tris^HCl, pH 7.8). The outlined BR trimer representing sections close to the cytoplasmic surface of the lipid membrane was obtained after merging six atomic models of BR.

At 200 pN AFM topographs changed: prominent EF loops (S.D. of 0.19 nm) bent away; shorter loops of the BR monomers were visualized. conformational change fully reversible suggesting that loop EF is flexible

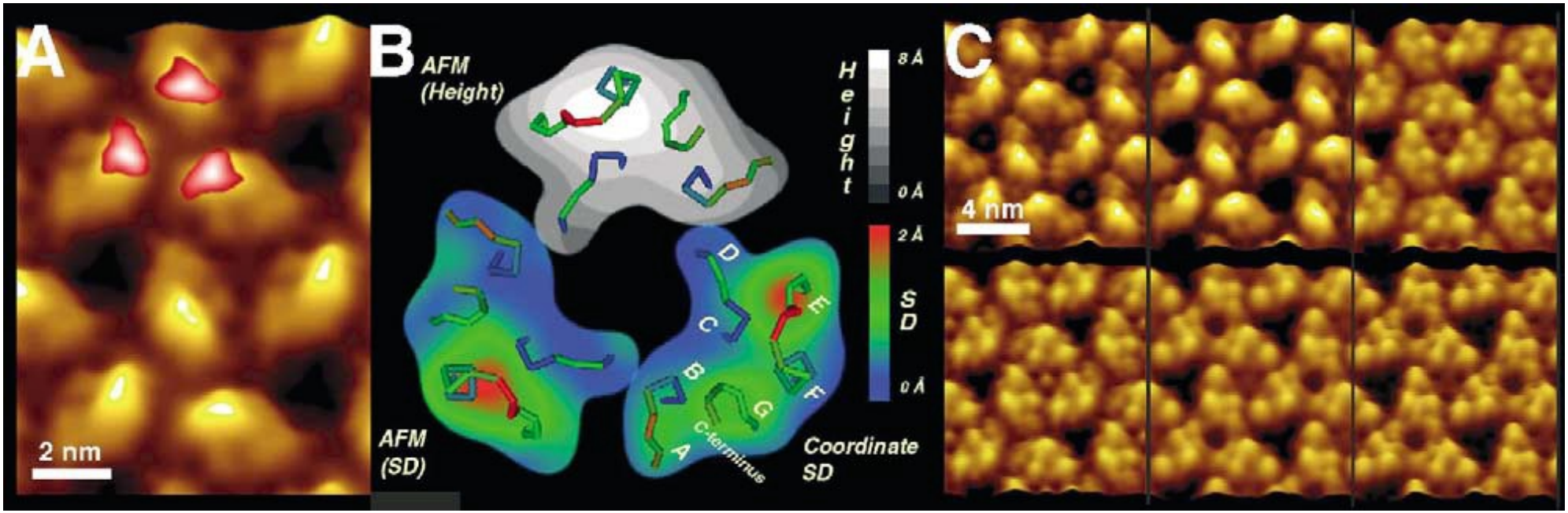

Fig. 16. Quantitative analysis of the native cytoplasmic purple membrane surface. (A) Correlation average of the AFM topograph recorded at an applied force of 100 pN (Müller et al., 1999b). Regions with enhanced flexibility are derived from SD maps and superimposed in red to white shades. (B) Different surface properties of bacteriorhodopsin. The surface loops are shown as backbone tracings colored according to the backbone coordinate root-mean-square deviation (SD) calculated after merging five different atomic models of bacteriorhodopsin (Heymann et al., 1999). The gray scale image shows the height map determined by AFM (A) with the prominent protrusion representing the EF loop. The colored monomers represent the SD between the atomic models, and of the height measured by AFM. (C) Unraveling the force induced structural changes of the cytoplasmic surface by multivariate statistical analysis. Top left: purple membrane imaged at 80 pN. Top center: same membrane imaged at approximately 100 pN. Top right: at about 150 pN the EF loop is bent away while the shorter polypeptide loops of the cytoplasmic surface become visible. Bottom row: three conformations differing in their central protrusion are observed at approximately 180 pN. Topographs exhibit a vertical range of 1 nm and are displayed as relief tilted by 5°.

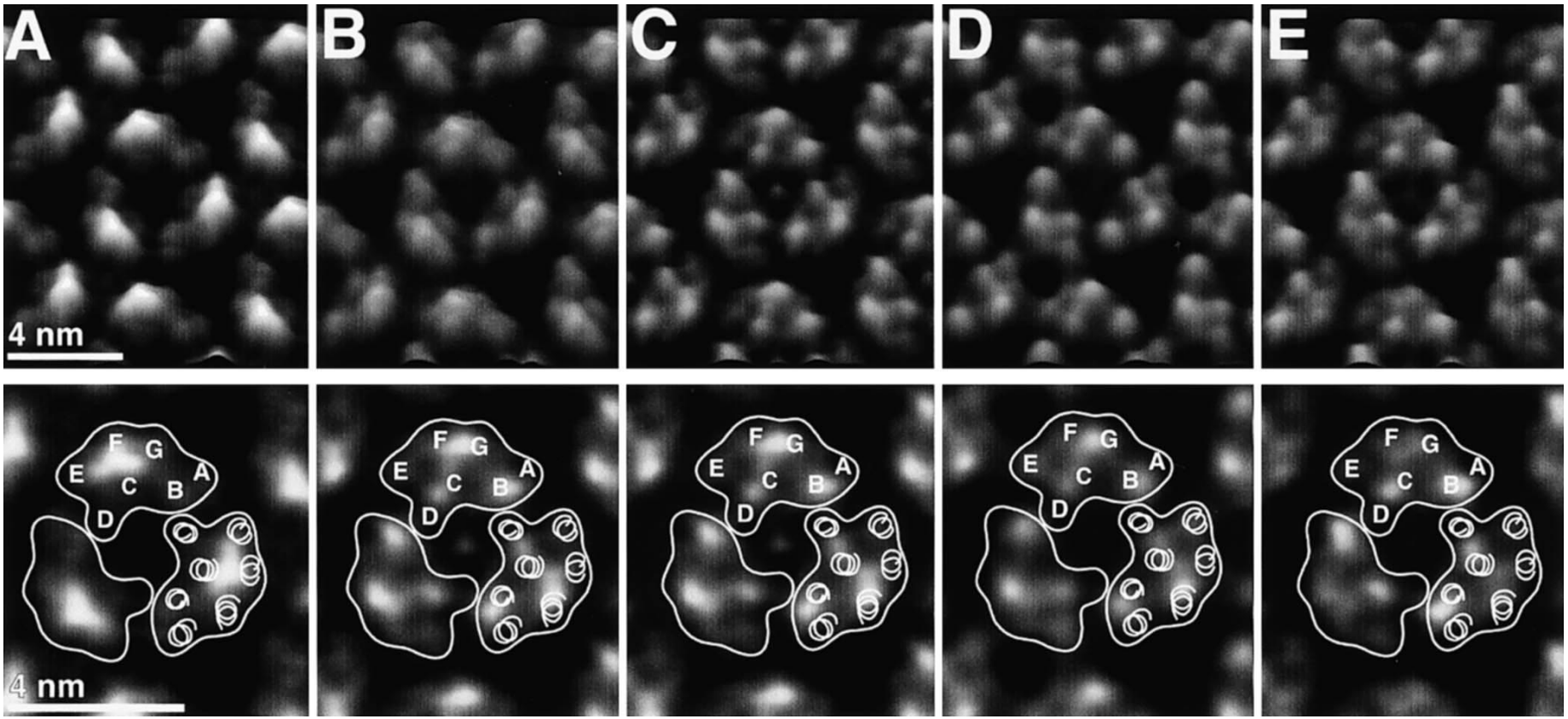

Structural variability of the native cytoplasmic purple membrane surface. The three-fold symmetrized averages were calculated from unit cells classifed by multivariate statistical analysis using the algorithm kindly provided by J.-P. Bretaudiere. (A) PM imaged at slightly enhanced forces of 120 pN (compare to Fig. 3B). Same membrane imaged at an applied force of approximately 150 pN (B). In C, D and E, three conformations of the membrane are imaged at approximately 180 pN. The last three averages differ in their central protrusion. The correlation averages are displayed in perspective view (top) and in top view (bottom) with a vertical brightness range of 1 nm.

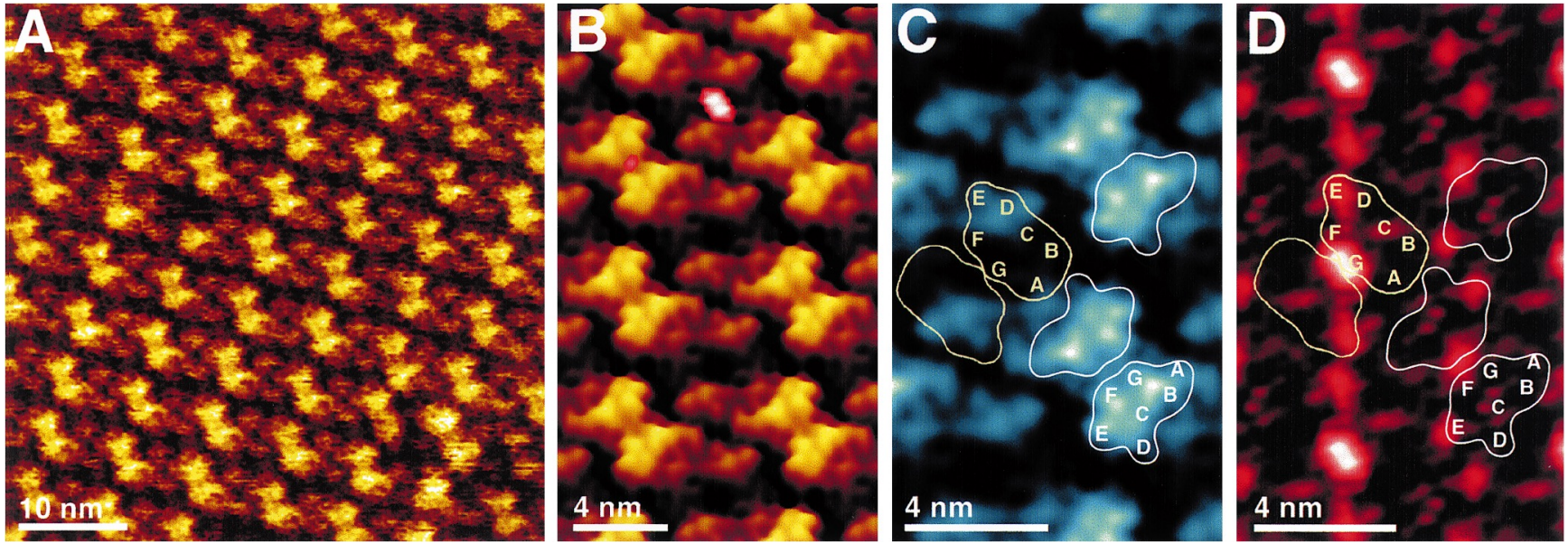

Recrystallization of BR in the presence of n-dodecyl trimethylammonium chloride (DTAC) yielded well-ordered 2D crystals that adsorbed flatly onto freshly cleaved mica. They had sizes of up to 5 nm, and a thickness of 5.8+-0.4 nm, which was slightly more than that of the native PM, 5.5 +-0.4 nm. Topographs of these orthorhombic crystals showed BR dimers assembled into a rectangular lattice with a p22121 symmetry and unit cell dimensions of a =5.8 nm, b=7.4 nm. Accordingly, the BR dimers alternately had their cytoplasmic surface or their extracellular surface facing the stylus. Surprisingly, it was not possible to induce conformational changes of the EF loops in this BR crystal form.
Increasing the applied force of the stylus resulted in a deformation of the whole protein surface rather than in the bending of a single loop, and reduced the lateral resolution. The observed structural changes suggest that the interactions of the cytoplasmic polypeptide loops depend on how the BR molecules associate.

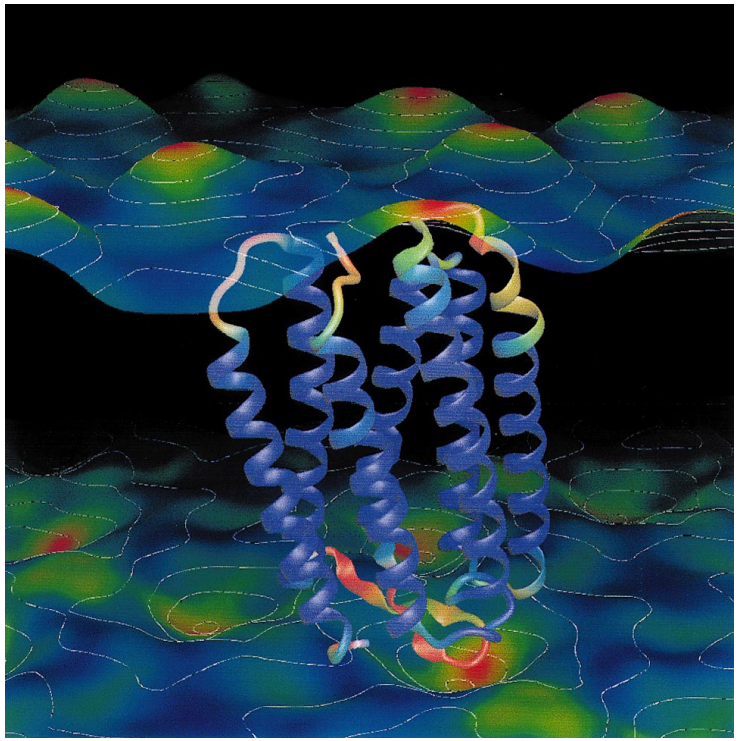

Information about the surfaces of BR have been derived from electron crystallography and Xray diffraction at high resolution, and AFM at medium resolution. This provided an excellent opportunity to assess the quality of the AFM topographs of the PM, and **to understand the implications of combining AFM data with the other structure determination methods**.
Six BR atomic models were combined and compared with the AFM data to determine the value and reliability of each source of information.
Fig. 6 shows one atomic model suspended within an envelope of the PM reconstructed from the AFM data. The ribbon diagram is color coded according to the coordinate variance between the different atomic models, while the surfaces are mapped with the AFM S.D. images. There is an excellent correspondence between the surface loops of the BR model and the AFM envelope.

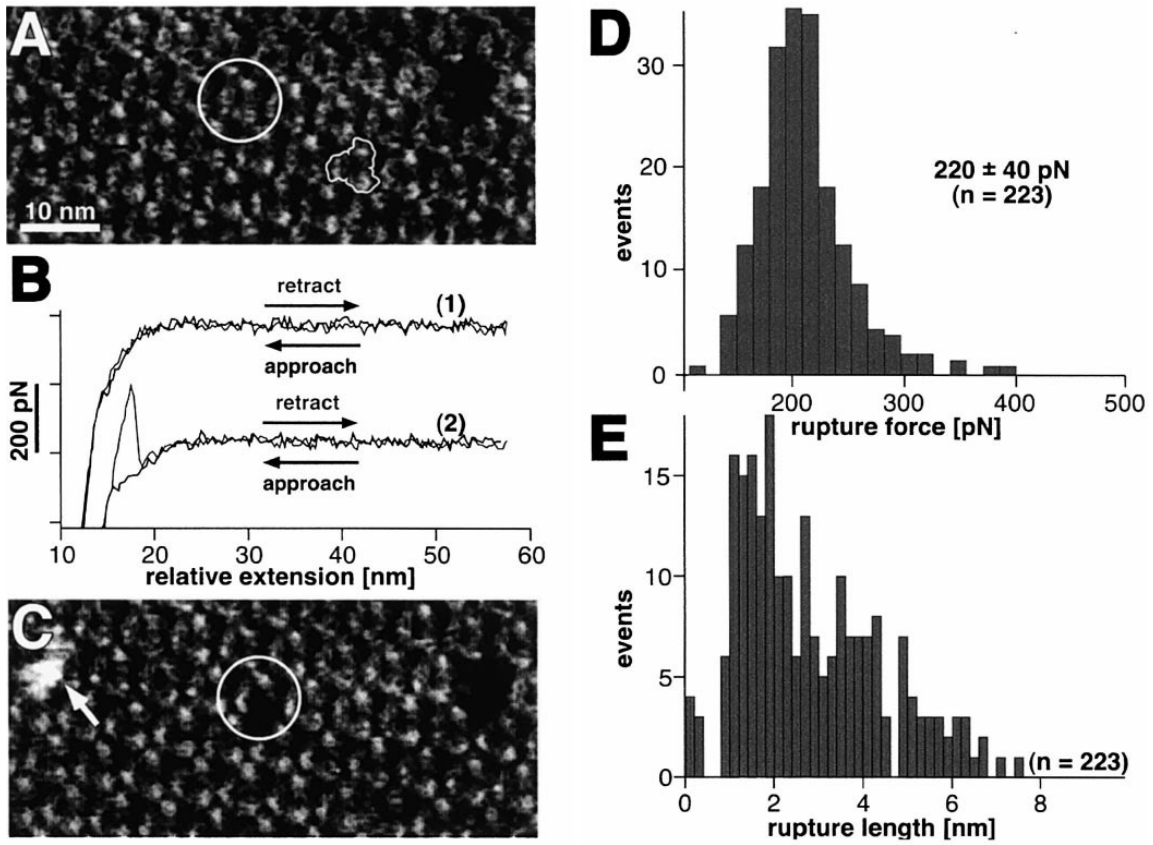

Extracting individual bacteriorhodopsins from native purple membrane. (A) AFM topograph of the cytoplasmic surface of PM recorded in buffer solution. The BR molecules forming trimers (outlined trimer) are clearly visible. (B) Most of the extension curves recorded on the cytoplasmic surface were unspectacular (1). However, 10% of the other extension curves showed one adhesion peak at a separation of several nm from the PM surface (2). The adhesion force of the peak shown in (2) was about 220 pN. (C) The topograph of the same surface imaged after recording the adhesive force peak showed one BR monomer missing (outlined circle). After extraction of the BR from the PM, a protrusion of about the size of an individual BR molecule was observed to be adsorbed onto the membrane surface (arrow). The missing trimer at the upper right was taken to align the topographs. Full gray level range of topographs, 1.5 nm. (D) Histogram of the rupture forces required to pull an individual BR from the PM. The average adhesion force was 220 fl 40 pN (n = 223). (E) Histogram of the pulling lengths until the BR molecules were extracted from the membrane.

Dynamics of bR on purple membranes

Ando's group, Angew Chem Int Ed, 2011

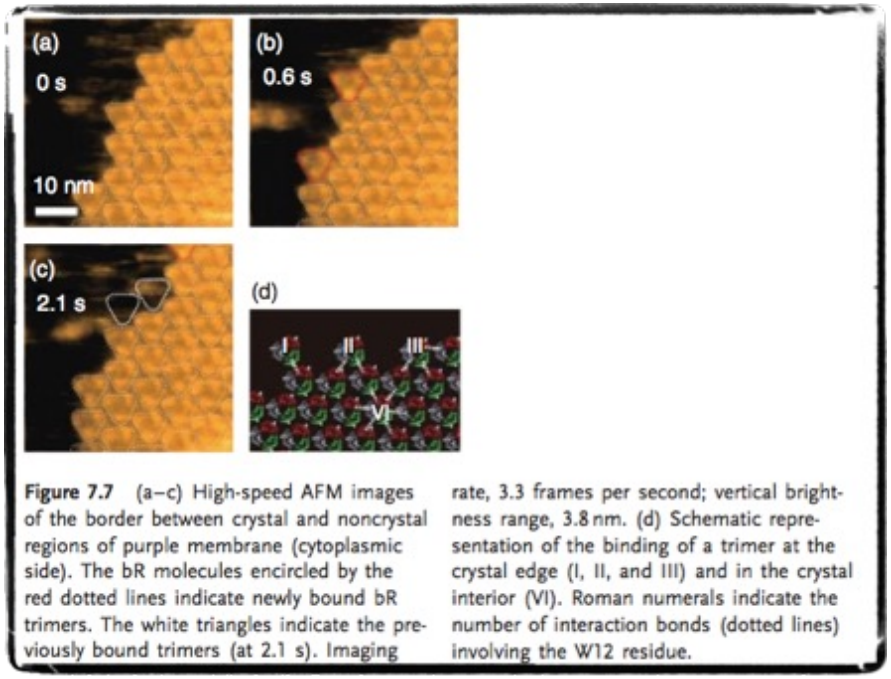

Figure 7.7 (a–c) High-speed AFM images of the border between crystal and noncrystal regions of purple membrane (cytoplasmic side). The bR molecules encircled by the red dotted lines indicate newly bound bR trimers. The white triangles indicate the previously bound trimers (at 2.1 s). Imaging rate, 3.3 frames per second; vertical brightness range, 3.8 nm. (d) Schematic representation of the binding of a trimer at the crystal edge (I, II, and III) and in the crystal interior (VI). Roman numerals indicate the number of interaction bonds (dotted lines) involving the W12 residue.

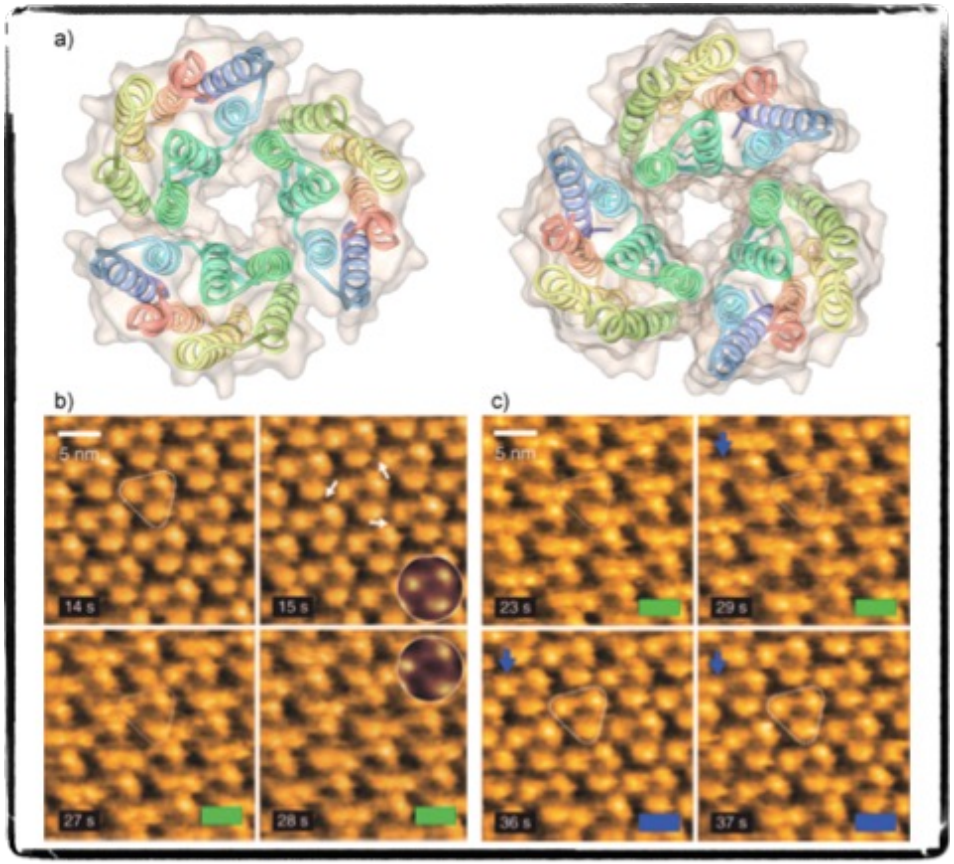

bR molecules with two binding partners associated for longer time periods to the array than proteins that had only one neighbor. Statistical assessment of the dissociation frequencies allowed the calculation of the **strength of a single bR–bR interaction of 1.5kBT (0.9 kcal/mol), resulting in a stability of about 5.4 kcal/ mol for the purple membrane arrays**, in good agreement with ensemble measurements by calorimetry

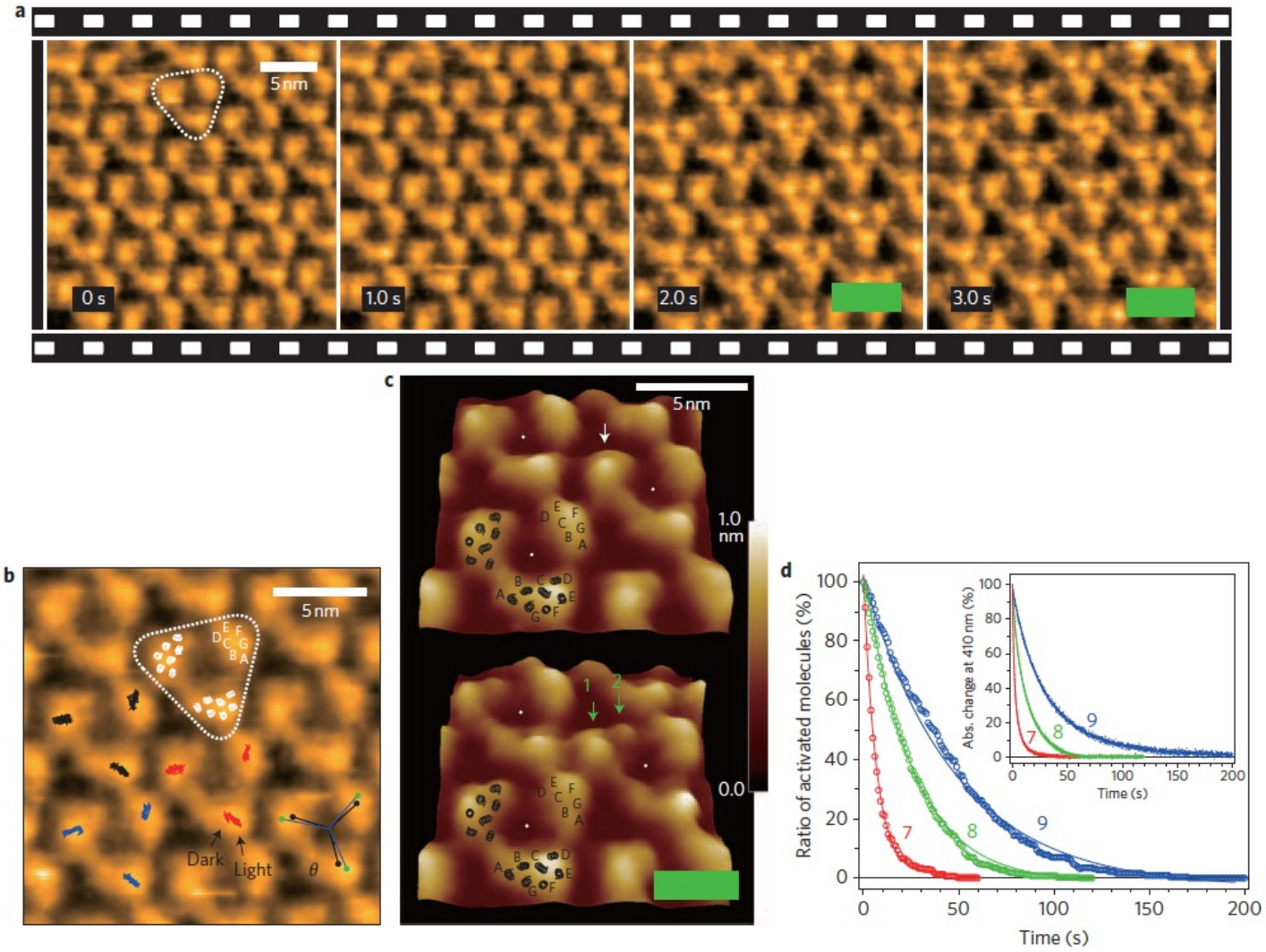

Figure 1 | High-speed AFM images of the cytoplasmic surface of D96N under dark or illuminated conditions. a, Successive AFM images of D96N bR adsorbed onto a mica surface in 10 mM Tris-HCl (pH 7) and 300 mM KCl. Frame rate, 1 fps; pixel size, 200 × 200 pixels (Supplementary Movie S1). A bR trimer is highlighted by the white triangle. The green bars indicate illumination of 532-nm green light at 0.5 μW. **b**, Traces (red, blue and black marks) of the mass centre positions under dark–illumination cycles are superimposed on the image of D96N in the dark. The photo-induced movement of bR includes counterclockwise rotation (7.4±2.2°) around the trimer centre. **c**, Surface maps of the magnified images in the dark (upper panel) and under illumination (bottom panel). The position of each trimer centre is denoted by white dots. A monomer in the dark is indicated by a single white arrow. Under illumination, the topography of the monomer splits into major and minor protrusions, as indicated by green arrows 1 and 2, respectively. **d**, Decay after flash-illumination of the activated state at different pH values (7, 8 or 9), detected by high-speed AFM. The exponential decay constants (τ) at pH 7, 8 and 9 are 6.7±0.10 s (the total number of analysed bR molecules, $n_T = 320$; the number of different molecules analysed, $n_m = 52$), 25±0.25 s ($n_T = 373$, $n_m = 65$), and 48±0.59 s ($n_T = 214$, $n_m = 120$), respectively. The inset shows the absorbance change at 410 nm (that is, decay of the M-intermediate) after flash-illumination of D96N measured at various values of pH (7, 8 or 9). The exponential decay constants (τ) at pH 7, 8 and 9 are 3.4±0.025 s, 14±0.034 s and 33±0.080 s, respectively.

Nature Nanotechnology 2010, M. Shibata…T. Ando

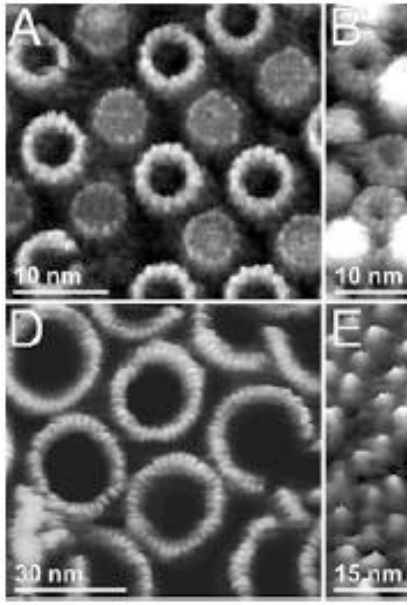

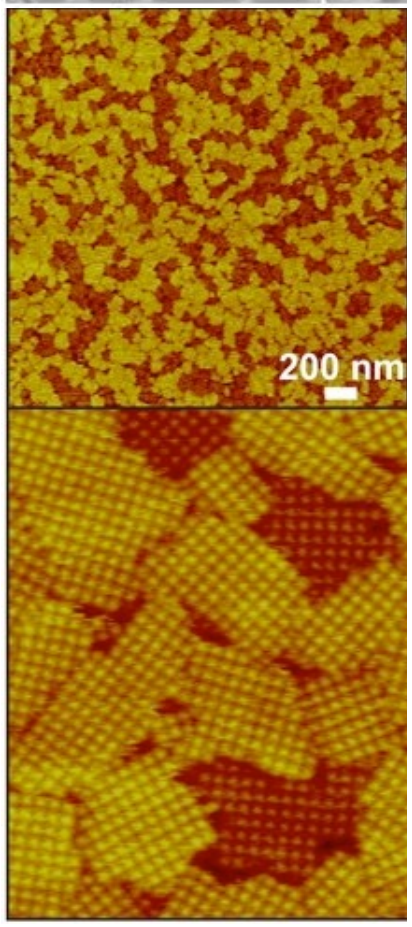

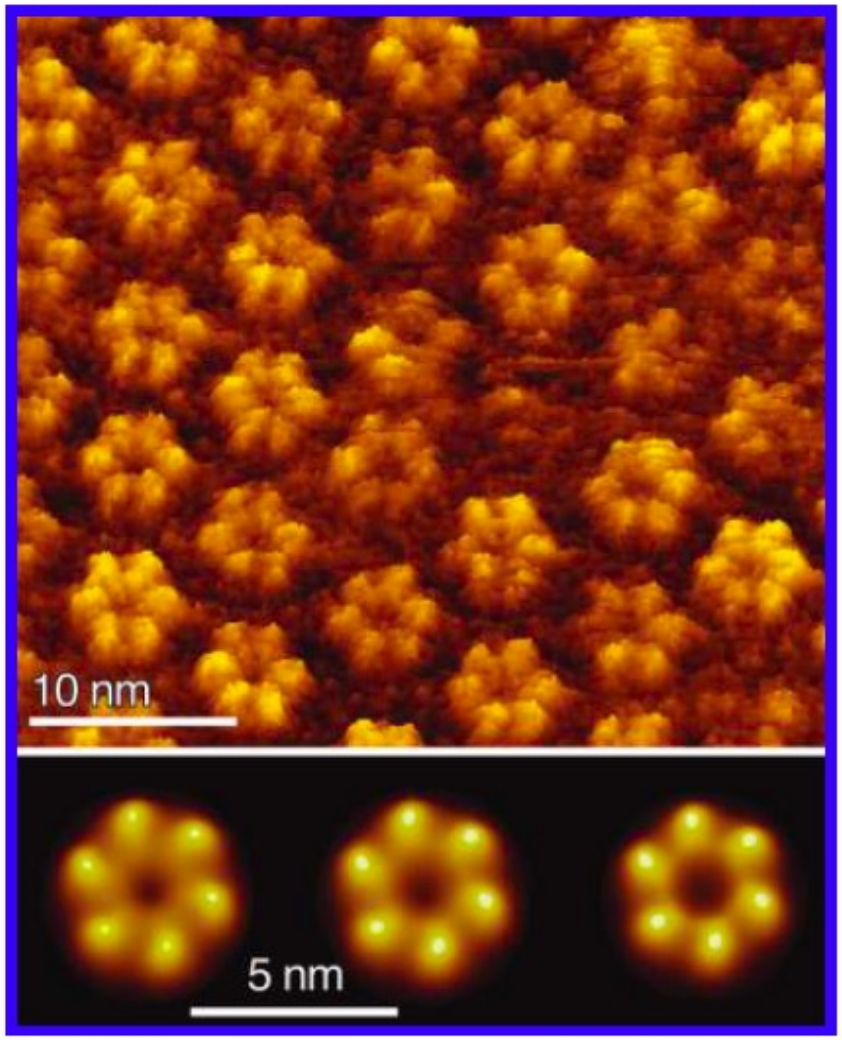

FIGURE 4: Watching communication channels at work. High-resolution AFM topograph showing the extracellular surface of Cx26 gap junction hemichannels. The gap junction membranes have been dissected with the AFM probe to expose their extracellular surface (*27*). The bottom row shows the conformational change of hemichannels in response to Ca^{2+}. The closed channels (left) switch, via an intermediate conformation (middle), to the open state (right) in the presence of 0.5 mM Ca^{2+}. Hemichannels in the bottom row represent correlation averages.

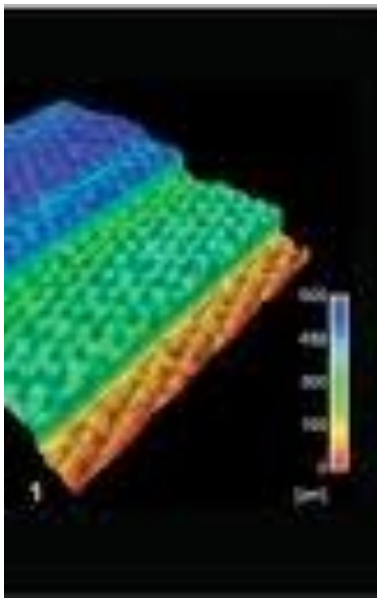

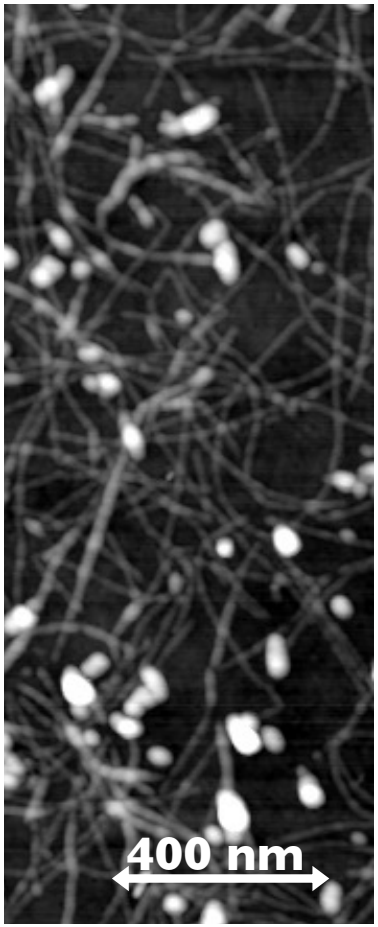

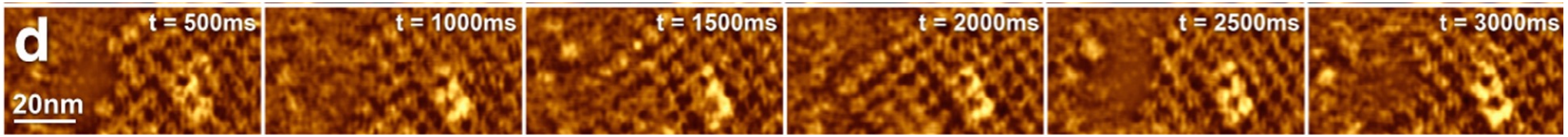

Using HS-AFM in contact mode, applying additional force s the junctional microdomains were dissected, revealing that the adhesion function of the proteins was cooperative: the entire membrane patches dissociated at once. From high spatial and temporal res. Assembly/dissasembly of auqaporin-0 and connexons to/from functional microdomains, with interaction strenght of -2.7 K_BT

HS-AFM on life cell

2.7 s/frame, with bright-field illumination

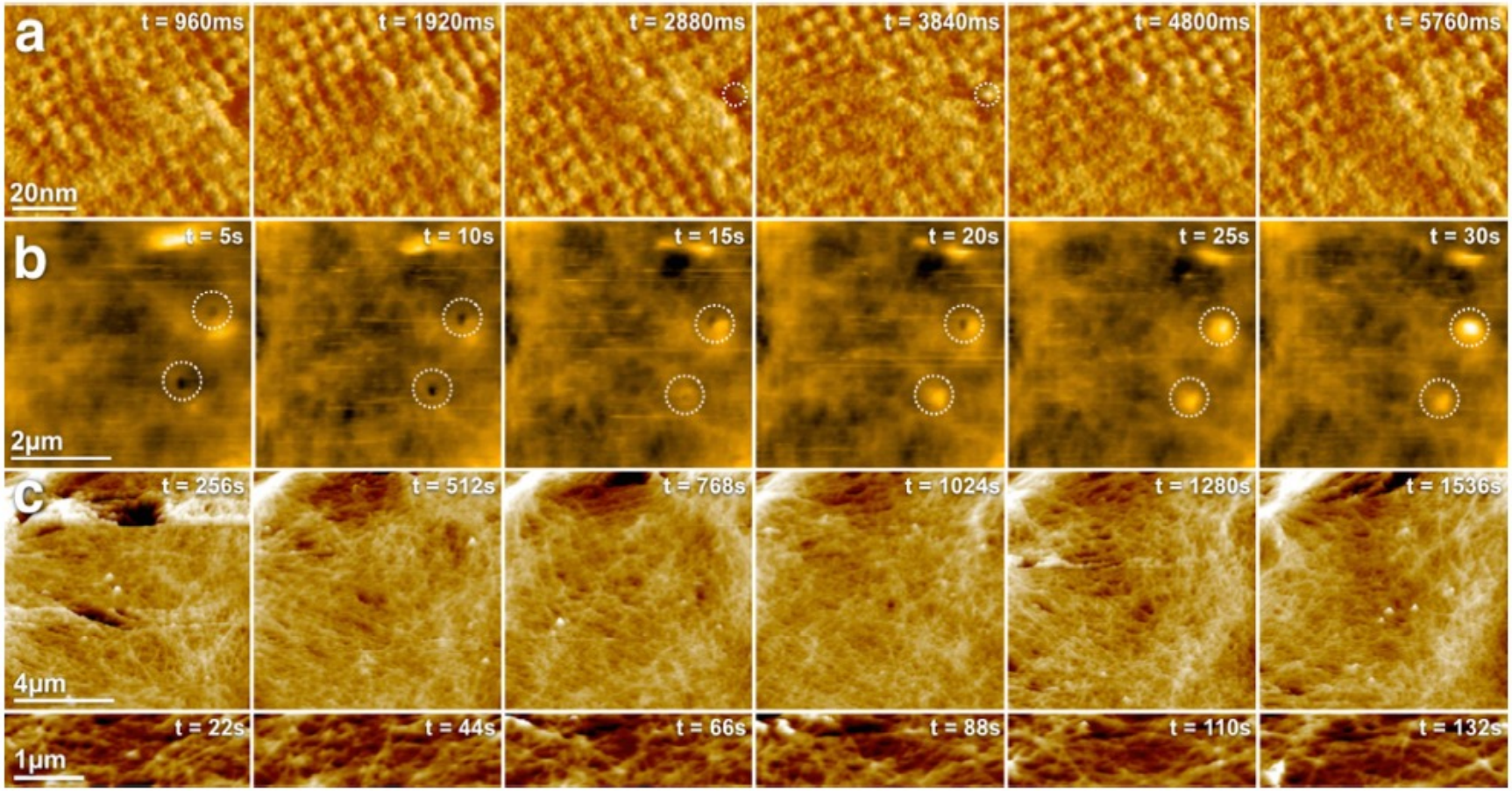

Fig. 2. HS-AFM applications on life cells. (a) High-resolution HS-AFM imaging of AQP0 in junctional microdomains in native eye lens cells. The dynamic association of individual AQP0 could be observed (outline). (b) Endocytosis events observed by HS-AFM on HeLa cells. (c) Dynamic PeakForce tapping imaging of the membrane cortex underneath the plasma membrane of 3T3 fibroblasts.

Colom, A., Casuso, I., Rico, F. and Scheuring, S. (2013) A hybrid high-speed atomic force–optical microscope for visualizing single membrane proteins on eukaryotic cells. Nat. Commun. 4.

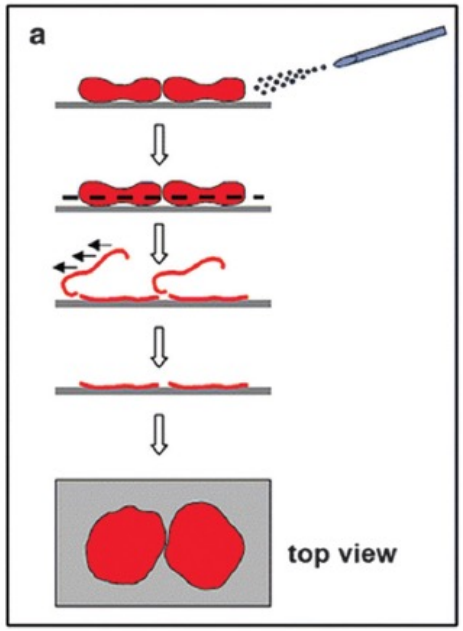

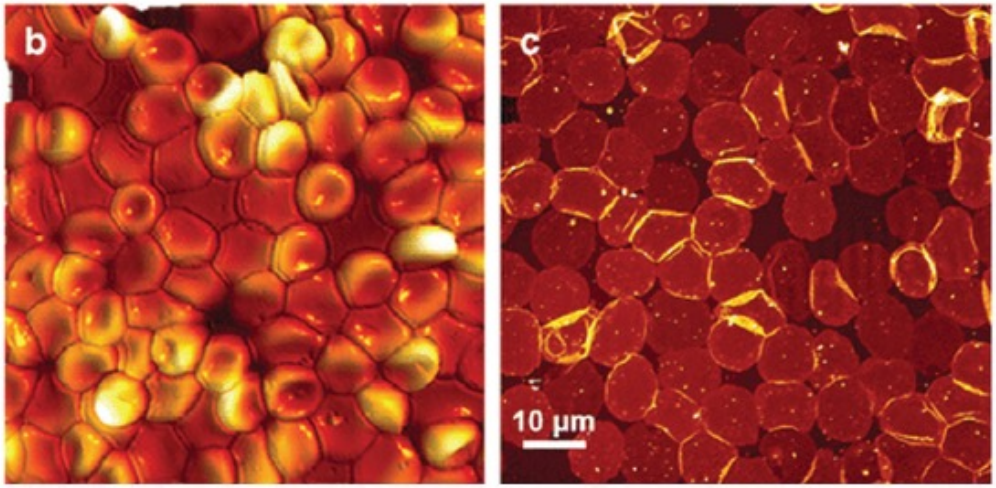

Fig. 11 Membrane preparation scheme. (a) RBCs are exposed to fluid flow-imposed shear stress to open the cells. (b) AFM images of RBCs attached to poly-L-lysine-coated glass. (c) Inside-out RBC membranes spread on the glass surface after shear stress. Adapted from ref. 91, Figure 1 with permission.

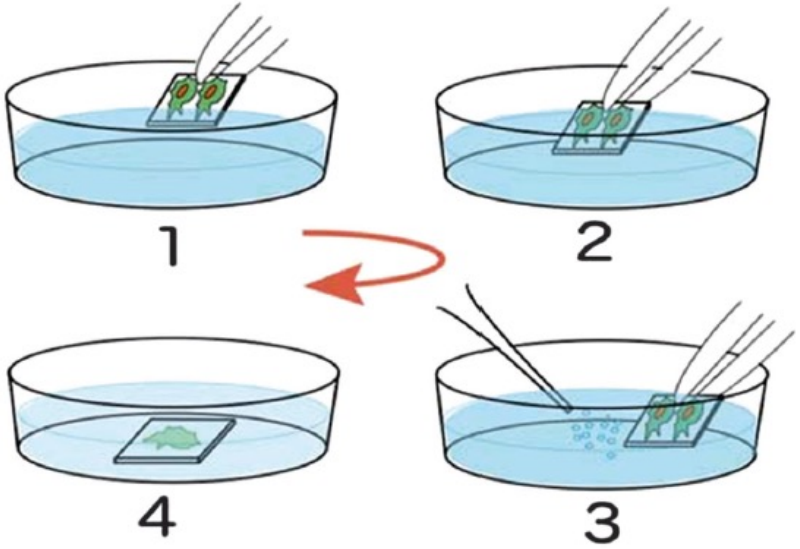

Fig. 12 Scheme for unroofing cells. The cells are washed three times in hypotonic HEPES-based mammalian Ringer's solution and subsequently unroofed by ultrasonic stimulation, which removes the apical cell membrane and the cytoplasm. Adapted from ref. 95, Figure 1 with permission.

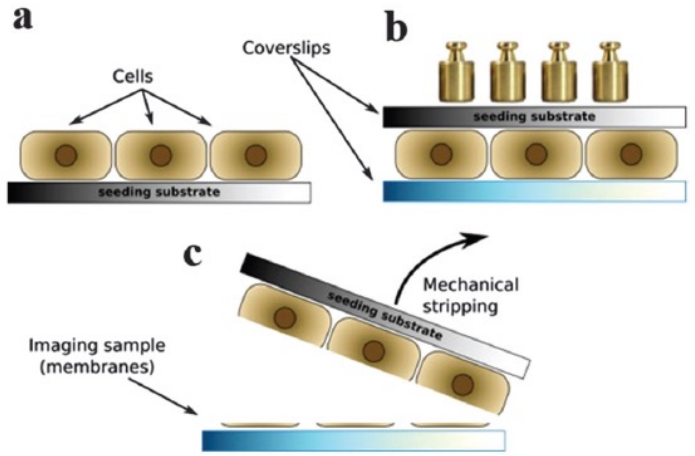

Fig. 13 Scheme of the preparation of the apical cytoplasmic side of membranes. (a) Cells are cultured on a seeding substrate. (b) A coverslip covers another side of the cells, and weights are placed on the seeding substrate. (c) Stripping the seeding substrate to leave the apical membranes for imaging. Adapted from ref. 97, Figure 1 with permission.

The $\alpha_3\beta_3\gamma$ subcomplex of F_1-ATPase (a part of ATP synthase) is the minimum complex for the full ATPase activity. About half the length of the long γ subunit is inserted into the central cavity formed by a ring-shaped $\alpha_3\beta_3$ where three α subunits and three β subunits are arranged alternately (1). Three ATP binding sites locate at the α-β interfaces, mainly in the β subunits. The $\alpha_3\beta_3\gamma$ subcomplex is a rotary motor (34, 48, 68, 115) (**Figure 5*a***). The γ subunit rotates in the stator $\alpha_3\beta_3$ ring driven by rotary hydrolysis of ATP at the three β subunits. The rotation occurs in the counterclockwise direction as viewed from the exposed side of the γ subunit (or from C-terminal side of $\alpha_3\beta_3$). In the ATPase cycle, three β subunits take different chemical states: ATP-bound, ADP-bound, and nucleotide-free (empty) states (1, 34). Each chemical state cyclically propagates over the three β subunits. Thus, there is strong cooperativity between β subunits.

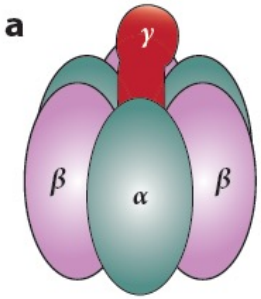

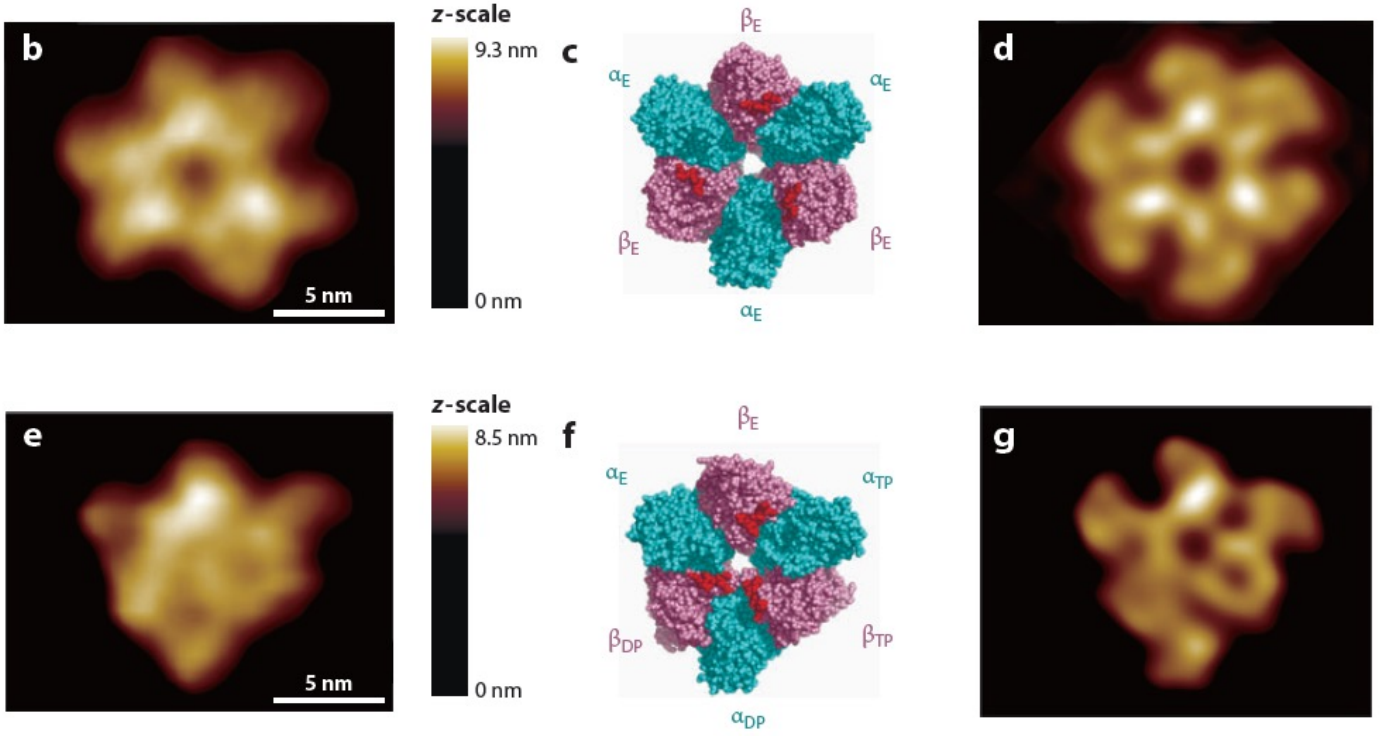

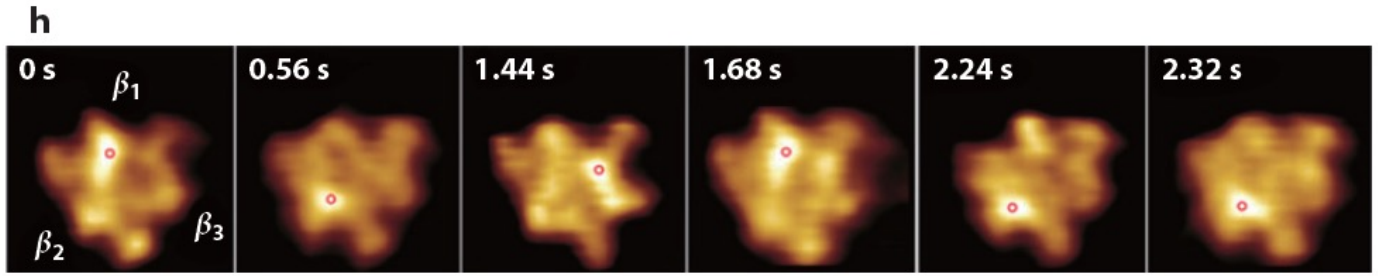

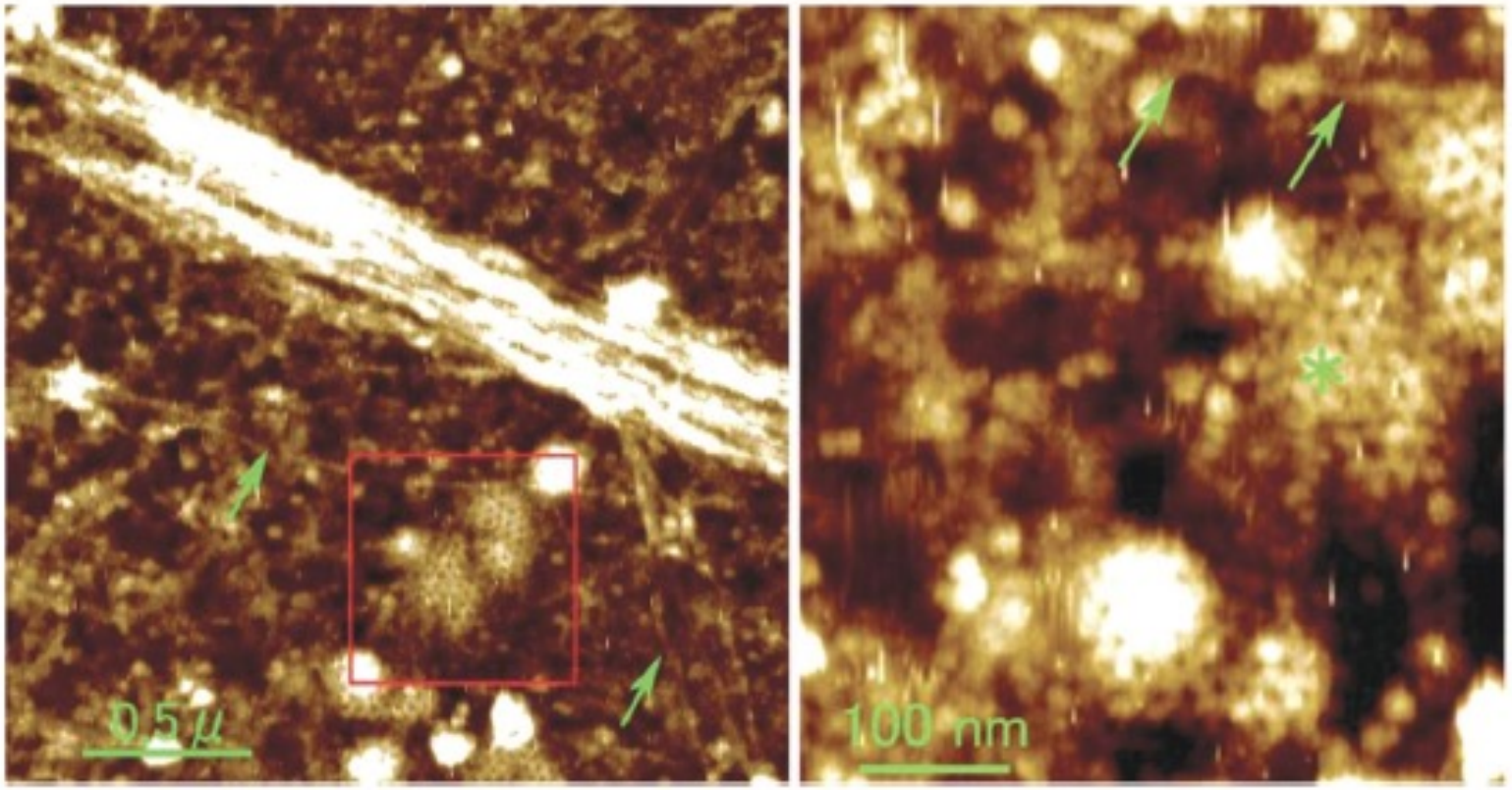

Fig. 18 AFM image of clathrin coats and actin filaments at the cytoplasmic surface of the plasma membrane. The right figure shows an enlarged view of the boxed area in the left figure. Clathrin-coated pits are clearly observed in the boxed area. Arrows indicate actin filaments. From ref. 95, Figure 6 with permission.

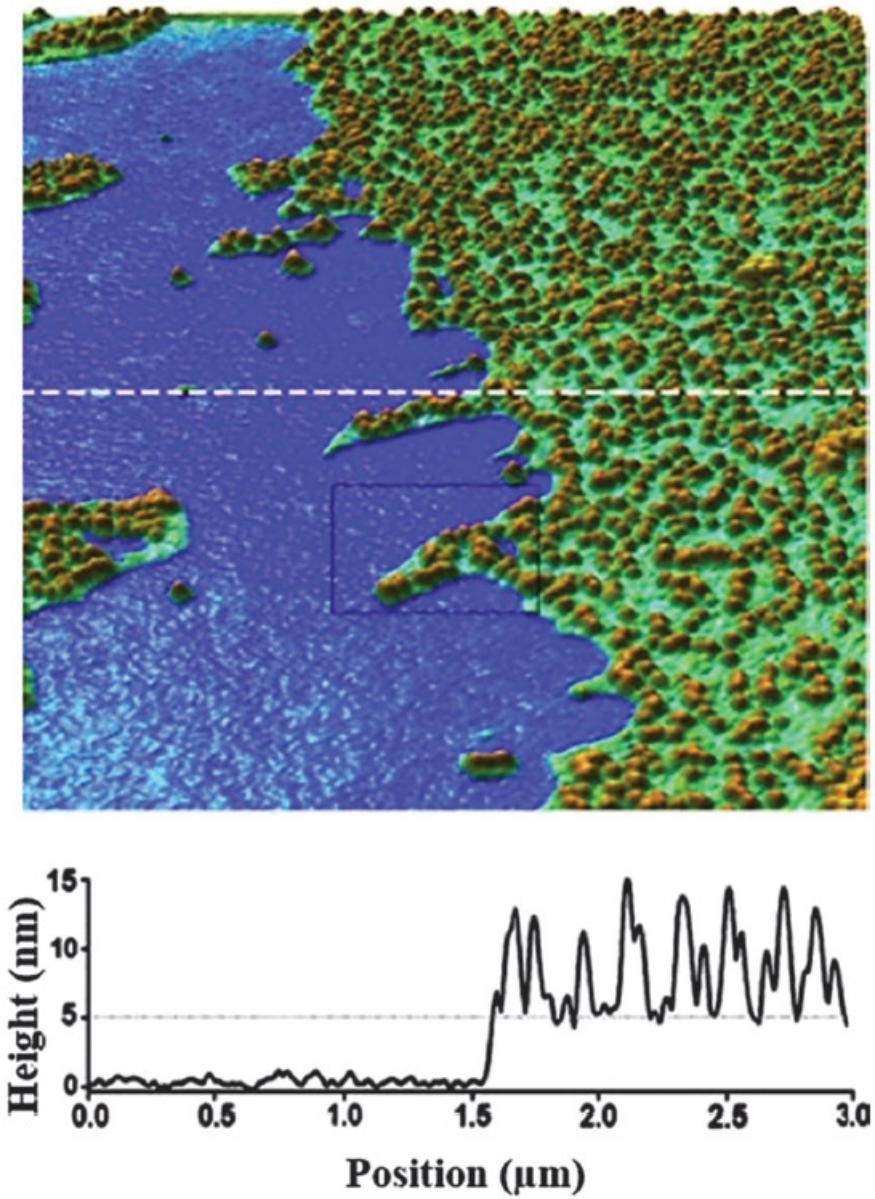

Fig. 17 AFM image of South African frog oocyte membranes (cytosolic side). Poly-L-lysine-coated glass (blue), the lipid bilayer membrane (turquoise), and the membrane proteins (brown). The height profile along the broken line is presented at the bottom. From ref. 91, Figure 6 with permission.